BIOCHEMISTRY
including biophysical chemistry & molecular biology

Article

pubs.acs.org/biochemistry

N-Terminus of IpaB Provides a Potential Anchor to the *Shigella* Type III Secretion System Tip Complex Protein IpaD

Nicholas E. Dickenson,[†] Olivia Arizmendi,[‡] Mrinalini K. Patil,[‡] Ronald T. Toth, IV,[§] C. Russell Middaugh,[§] William D. Picking,[‡] and Wendy L. Picking*[,‡]

[†]Department of Chemistry and Biochemistry, Utah State University, Logan, Utah 84322, United States

[‡]Department of Microbiology and Molecular Genetics, Oklahoma State University, Stillwater, Oklahoma 74078, United States

[§]Department of Pharmaceutical Chemistry, Macromolecule and Vaccine Stabilization Center, University of Kansas, Lawrence, Kansas 66047, United States

Supporting Information

ABSTRACT: The type III secretion system (T3SS) is an essential virulence factor for *Shigella flexneri*, providing a conduit through which host-altering effectors are injected directly into a host cell to promote uptake. The type III secretion apparatus (T3SA) is composed of a basal body, external needle, and regulatory tip complex. The nascent needle is a polymer of MxiH capped by a pentamer of invasion plasmid antigen D (IpaD). Exposure to bile salts (e.g., deoxycholate) causes a conformational change in IpaD and promotes recruitment of IpaB to the needle tip. It has been proposed that IpaB senses contact with host cell membranes, recruiting IpaC and inducing full secretion of T3SS effectors. Although the steps of T3SA maturation and their external triggers have been identified, details of specific protein interactions and mechanisms have remained difficult to study because of the hydrophobic nature of the IpaB and IpaC translocator proteins. Here, we explored the ability for a series of soluble N-terminal IpaB peptides to interact with IpaD. We found that DOC is required for the interaction and that a region of IpaB between residues 11−27 is required for maximum binding, which was confirmed in vivo. Furthermore, intramolecular FRET measurements indicated that movement of the IpaD distal domain away from the protein core accompanied the binding of $IpaB^{11-226}$. Together, these new findings provide important new insight into the interactions and potential mechanisms that define the maturation of the *Shigella* T3SA needle tip complex and provide a foundation for further studies probing T3SS activation.

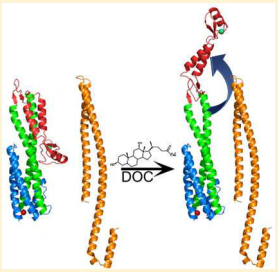

Shigella species cause a severe form of bacillary dysentery (shigellosis) that is readily spread via contaminated water. Shigellosis is of worldwide public health importance, with an estimated 90 million cases and 100 000 deaths per year with especially high incidence in children in low-income countries.[1,2] Those children that survive suffer impaired growth because of malnutrition, which is exacerbated by repeated episodes.[3] Shigellosis outbreaks also occur on a regular basis in industrialized nations, and the emergence of antibiotic resistant strains underscores the necessity to understand better the virulence mechanism of *Shigella*.[4]

Shigella employs a type III secretion system (T3SS) as its primary virulence factor.[5] The type III secretion apparatus (T3SA) resembles a nanosyringe and needle and provides a physical link between the *Shigella* and the gastrointestinal epithelial cell.[5] It is composed of three main components: the basal body, which spans the inner and outer bacterial membranes, serves as an anchor for the apparatus, and provides a conduit through the bacterial envelope; an external needle, with an outer diameter of 7 nm and a 2.5 nm inner channel, consisting of multiple copies of a MxiH packed in a helical manner;[6] and an exposed tip complex consisting of a pentamer of invasion plasmid antigen D (IpaD).[7,8] IpaD serves as a sensor of environmental small molecules, such as bile salts, to control the context of the tip complex and the secretion of effector proteins. Exposure to the bile salt dexoycholate (DOC) promotes recruitment of the first hydrophobic translocator, IpaB, to the maturing tip complex, where an organized oligomer forms the translocon prepore.[9,10] From this exposed position, it has been proposed that IpaB can sense host-membrane components, triggering recruitment of the second hydrophobic translocator, IpaC, to the *Shigella* exterior.[11] This completes formation of the translocon pore in the host cell membrane and induces secretion of T3SS host-altering effectors into the cell to promote pathogen entry.[11]

Although *Shigella* has provided a valuable system for identifying the steps encompassing T3SA tip complex maturation, the precise mechanisms and protein interactions that govern this process remain unknown. Recent studies have started to unravel some of these mechanisms by identifying an IpaD conformational change that occurs upon DOC binding. It has been proposed that this conformational change allows IpaB access to the maturing needle tip, where it associates with IpaD.[12,13] To date, verifying a direct association between IpaD and IpaB has been challenging, in part because of the

Received: June 13, 2013
Revised: November 13, 2013
Published: November 15, 2013

   dx.doi.org/10.1021/bi400755f | *Biochemistry* 2013, 52, 8790−8799

requirement of detergent to maintain soluble IpaB under aqueous conditions.

Previously, we generated stable IpaB N-terminal fragments that could be expressed in the absence of the cognate IpaB chaperone IpgC and are highly soluble in aqueous conditions.[14,15] In this study, we used these and additional IpaB fragments to explore conditions that may allow their stable interaction with purified IpaD. Fluorescence polarization (FP) and Förster resonance energy transfer (FRET) were employed to demonstrate that specific N-terminal fragments of IpaB are capable of binding with strong affinity to IpaD in a DOC-dependent manner. Furthermore, we found that a short peptide sequence located near the N-terminus of IpaB is necessary for optimal binding. This region has recently been identified as one of two likely binding domains important for IpaB association with its chaperone IpgC,[15,16] suggesting that there is a direct competition for binding at this site by IpaD and IpgC within the bacterial cytoplasm. Intramolecular FRET measurements revealed a relationship between DOC binding, flexibility within the IpaD distal domain, and the interaction between IpaD and IpaB. Overall, these data provide the first direct evidence of an IpaD−IpaB interaction in vitro and valuable mechanistic insight into this interaction. Generation of several N-terminal mutations in wild-type IpaB provided a correlation between the in vitro binding studies and virulence *Shigella* phenotypes in vivo. The resulting findings suggest that regions near the N-terminus of IpaB are necessary for its interaction with IpaD and the sequential maturation of the T3SA needle tip. As the first step in T3SA tip-complex maturation and a prerequisite for the ability of *Shigella* to invade host cells, determining the biochemical basis for the interaction between IpaD and IpaB provides a valuable contribution toward understanding the molecular basis for the onset of type III secretion induction in *Shigella* with ramifications that extend to related T3SSs. This could, in turn, help in the development of anti-infective measures against not only *Shigella* but also other important pathogens that rely upon type III secretion as an essential component of their virulence arsenals.

EXPERIMENTAL PROCEDURES

Materials. *Shigella flexneri ipaB*-null strain SF620 was provided by P. J. Sansonetti (Pasteur Institute, France).[17] *Escherichia coli* strains, protein expression plasmids, and Clonables 2× ligation premix were from Novagen (Madison,-WI). Restriction enzymes were from New England Biolabs (Ipswich, MA). Alexa Fluor probes, fluorescein maleimide (FM), 7-diethylamino-3-(4′-maleimidylphenyl)-4-methylcoumarin (CPM), and FlAsH-EDT$_2$ were from Invitrogen (Carlsbad, CA). Oligonucleotide primers were purchased from Integrated DNA Technologies (Coralville, IA). Iminodiacetic acid−sepharose was from Sigma Chemical Company (St. Louis, MO). All other solutions and chemicals were reagent grade.

Plasmid Constructs and Expression of *ipaB* and *ipaD*. Wild-type *ipaD* and *ipaD* made to encode a tetracysteine binding pocket (amino acid sequence CCPGCC) within the distal domain were produced as described previously.[13] The N-terminal IpaB peptides were generated in plasmid pT7HMT or a modified version of the plasmid that introduced an N-terminal cysteine and expressed as previously described.[14,18] Mutations encoding the IpaB internal cysteine point mutants used for FRET were introduced into both full-length *ipaB* and *ipaB*$^{11-226}$ using 5′ phosphorylated primers and inverse PCR. Residues 107, 120, 128, and 149 were chosen because they provide a mild mutation from serine to cysteine and all reside within the backbone of the solved IpaB$^{74-224}$ structure. For phenotypic characterization, the *ipaB* cysteine point mutants and deletion mutants were generated in plasmid pWPsf4, which was electroporated into the *S. flexneri ipaB*-null strain SF620. For protein expression, the cysteine mutants generated in *ipaB*$^{11-226}$ were cloned into pT7HMT, and the IpaB N-terminal deletion mutants were subcloned into pET15b. The N-terminal IpaB fragments containing an N-terminal cysteine were generated using a modified version of the pT7HMT expression plasmid.[18] The resulting plasmids were introduced into *E. coli* Tuner(DE3). All of the *E. coli* Tuner(DE3) strains were grown at 37 °C in terrific broth to an OD_{600} of 1.0, protein expression was induced with 1 mM IPTG for 18 h at 17 °C, and the recombinant protein was purified using standard nickel-chelation chromatography as previously described.[14]

Characterization of Novel IpaB Peptides and Mutants. The secondary structures and thermal stabilities of IpaB$^{1-226}$ and IpaB$^{28-226}$ were previously published.[15] The intermediate peptide, IpaB$^{11-226}$, the IpaB N-terminal deletion mutants, and the four cysteine point mutants generated for this study were also analyzed by far-UV CD using a Jasco Model J-815 spectropolarimeter equipped with a Peltier temperature controller (Jasco Inc., Easton, MD). Secondary-structure content was assessed by collecting CD spectra from 190 to 260 nm at 10 °C using a 0.1 cm quartz cuvette. A scanning rate of 50 nm/min was used with a spectral resolution of 0.2 nm and a 2 s data-integration time. All spectra are an average of three measurements. The proteins' secondary-structure thermal stability was determined by monitoring the CD signal at 222 nm over a temperature range from 10 to 90 °C. The CD signal was acquired every 2.5 °C as the temperature was increased at a rate of 15 °C/h and maintained at each interval for 1 min to allow the solution temperature to equilibrate. The protein concentration was 0.3−0.5 mg/mL in 10 mM phosphate (pH 7.4) with 150 mM NaCl (PBS) for all proteins, and measurements were normalized by converting the output signal to mean residue molar ellipticity.

Phenotypic Characterization of IpaB Mutants. Three independent assays were used to characterize the effect of IpaB mutations.[8] First, the effect of the IpaB mutations on the invasive capacity of *Shigella* was monitored using HeLa cells in a standard gentamycin protection assay using SF620 expressing wild-type *ipaB* as the positive control (100% invasion). Second, the ability of *Shigella* to form a translocon pore through proper recruitment of the translocator proteins IpaB and IpaC can be determined by contact-mediated hemolysis. SF620 expressing the IpaB mutants were tested for their contact hemolytic activity and compared to SF620 expressing wild-type *ipaB* (100% contact-mediated hemolysis). Third, uninduced secretion profiles measure the T3SA control of secretion during regular growth. The uninduced secretion of IpaD, IpaB, and IpaC into the culture media during overnight growth was assessed by western blotting. Blots were probed with a primary antibody mixture containing mouse anti-IpaD, rabbit anti-IpaB, and rabbit anti-IpaC polyclonal antibodies and the corresponding Alexa Fluor 680 goat anti-rabbit IgG and Alexa Fluor 800 goat anti-mouse IgG (Molecular Probes, Eugene, OR). Images were obtained using an Odyssey Infrared Imager (LI-COR, Lincoln, NE).

Labeling of Recombinant Protein with Fluorescent Probes. The N-terminal cysteine introduced into IpaB

peptides or the corresponding internal cysteine in the IpaB$^{11-226}$ point mutants were fluorescently labeled with FM. The purified proteins were dialyzed into 50 mM HEPES (pH 7.2), 140 mM NaCl, and 2.5 mM TCEP and degassed under N_2. FM prepared in *N*′,*N*′-dimethylformamide (DMF) was added to approximately a 10 molar excess to an aliquot of the protein and allowed to react for 2 h at room temperature under N_2. The unbound dye was removed by nickel-chelation chromatography, and the labeled protein was eluted and dialyzed into PBS. The native cysteine of IpaD (residue 322) was labeled with the thiol-reactive 7-diethylamino-3-(4′-maleimidylphenyl)-4-methylcoumarin (CPM) as described previously.[19] Protein secondary structure and thermal stability were verified by far-UV CD spectroscopy. Because of interference with CD signals after fluorescence labeling, the retention of structural features for labeled IpaB fragments was determined by Fourier-transform infrared (FTIR) spectroscopy. The infrared spectrum of each sample was collected at room temperature using a Vertex 70 FTIR spectrometer (Bruker Corp., Billerica, MA) using a BioATR cell (Harrick Scientific, Pleasantville, NY). The data were collected from 256 composite scans over a range of 4000 to 900 cm^{-1} with a resolution of 4 cm^{-1}.

For the intramolecular FRET analysis, the CCPGCC tetracysteine motif introduced into the distal domain of purified IpaD was labeled with FlAsH-EDT_2 (a biarsenical fluorescein reagent that coordinates with the above tetracysteine motif) as described previously.[13] Both the donor-only FlAsH-labeled IpaD and the donor and acceptor doubly labeled IpaD were dialyzed into PBS and used within 1 week or stored at −80 °C.

Fluorescence Polarization. The FM-labeled N-terminal cysteine mutants of IpaB$^{1-226}$, IpaB$^{11-226}$, and IpaB$^{28-226}$ were diluted to 80 nM in PBS, and IpaD was titrated in at concentrations from 0 to 10 μM. The mixtures were incubated for 30 min at room temperature, and the fluorescence polarization of the IpaB-bound fluorescein was measured using a Molecular Devices SpectraMax M5 fluorescence plate reader equipped with excitation and emission polarizers. The polarization was measured in 96-well opaque plates using an excitation wavelength of 490 nm and emission wavelength of 527 nm. The measurements were repeated following the addition of either 1 mM DOC or the synthetic bile salt dehydrocholate (DHC). These measurements were also used to test the binding of the IpaB$^{11-226}$ peptide to the IpaD homologues SipD (from *Salmonella enterica*)[20] and LcrV (from *Yersinia pestis*).[21] SigmaPlot 11.2 was used to plot the change in polarization as a function of IpaD (or homologue) concentration, and the data were fit to a single-site saturation ligand-binding equation to estimate the dissociation constant (K_d) for each interaction.

Förster Resonance Energy Transfer (FRET) Measurements. Fluorescence emission spectra of the FRET systems were collected at 20 °C with a FluoroMax-4 spectrofluorometer (HORIBA Jobin Yvon, Edison, NJ) (see ref 22 for a detailed description of FRET). For the detection of intermolecular FRET between IpaD and the IpaB$^{11-226}$ cysteine point mutants, the excitation wavelength was 385 nm (specific for the coumarin donor), and emission was collected from 400 to 600 nm with an integration time of 0.05 s. Donor-labeled IpaD (125 nM) was incubated with 1 μM of each IpaB$^{11-226}$ cysteine mutant either labeled with a fluorescein FRET acceptor (DA) or not (D only). Fluorescence emission spectra were collected for both conditions prior to and following a 30 min incubation with 1 mM DOC at 20 °C to observe the effects of DOC on the IpaD−IpaB interaction. Intramolecular FRET measurements between the acceptor-labeled native cysteine in IpaD and the donor-labeled tetracysteine binding pocket engineered into the distal domain were acquired similarly using an excitation wavelength of 485 nm (specific for the FlAsH donor), and emission was collected from 500 to 650 nm with an integration time of 0.05 s. Spectra were collected for 125 nM solutions of both IpaD labeled only with the FlAsH donor (D only) and IpaD dual labeled with the FlAsH donor and the Alexa 568 acceptor (DA). The IpaD was split and incubated for 30 min with either a PBS control or 1 mM DOC in PBS at 20 °C prior to titrating in IpaB$^{11-226}$ to 5 μM. The resulting data points were fit to a Hill1 binding model used to estimate the K_d of the interaction.

Calculating Energy-Transfer Efficiencies between FRET Pairs. FRET efficiencies were measured spectrophotometrically, as described above, and calculated by quantifying the reduction in donor fluorescence intensity when in the presence of an acceptor.[13,15] For this method, it is important that the donor concentration and labeling efficiency remain identical in the conditions of donor only and donor in the presence of acceptor to ensure that the change in observed donor fluorescence intensity is solely because of FRET. This was achieved for the intermolecular FRET measurements because either acceptor-labeled or nonlabeled ligand is added to the donor-labeled protein, ensuring that the donor conditions remain unchanged. For intramolecular FRET measurements, this is accounted for because the donor-only sample was split just prior to labeling of the protein with the FRET acceptor. Thus, for both techniques, the labeling efficiencies of the donor-only and donor−acceptor conditions are identical, and the energy-transfer efficiencies can be calculated by

$$E = 1 - (F_{DA}/F_D) \quad (1)$$

where E is the energy-transfer efficiency, F_D is the peak donor fluorescence intensity in the absence of the FRET acceptor, and F_{DA} is the peak donor fluorescence intensity in the presence of the FRET acceptor.[23] Because the energy-transfer efficiency is sensitive to the distance separating the FRET pair, comparing these efficiencies provides insight into changes in the spatial relationship between the donor and acceptor.

In Vivo *Shigella* Surface Localization of IpaB. The ability of IpaB mutants to localize stably to the tip of the T3SA was determined by flow cytometry. *Shigella* were grown to an OD_{600} of 0.4 prior to the addition of 1 mg/mL of DOC to the cultures. The bacteria were allowed to grow for an additional 30 min, collected by centrifugation, washed with PBS, and fixed by resuspension in freshly prepared 4% paraformaldehyde in PBS. The fixed cells were rinsed, diluted to ~5×10^8 bacteria/mL, and blocked with a 1:1 mixture of Odyssey blocking buffer/PBS prior to addition of appropriate primary antibodies. The samples were incubated at room temperature for 2 h, rinsed, and incubated with Alexa Fluor 488-conjugated goat anti-rabbit secondary IgG for 1 h, rinsed again, and diluted in PBS. The samples were then analyzed using a FACSCalibur flow cytometer set to collect 500 000 events for each mutant (BD Biosciences, San Jose, CA). The results were plotted and analyzed using FlowJo V10.0.6 (Tree Star, Ashland, OR).

RESULTS

Deoxycholate Promotes an Interaction between IpaD and N-Terminal IpaB Peptides in Vitro. Previous protease-digestion studies identified several stable core fragments of the highly hydrophobic *Shigella* translocator IpaB.[14] Most of the stable regions clustered near the IpaB N-terminus, with $IpaB^{28-226}$ being used to solve a 2.1 Å structure for $IpaB^{74-224}$.[14] Insights from this structure and the generation of soluble IpaB peptides capable of being expressed in the absence of IpgC have played an important role in dissecting interactions between IpaB and IpgC.[15] In this study, the cysteine residues introduced at the N-terminal extremity of the stable IpaB fragments $IpaB^{1-226}$, $IpaB^{11-226}$, and $IpaB^{28-226}$ were covalently labeled with a fluorescent probe to allow the use of fluorescence polarization (FP) to identify conditions that would permit their interaction with IpaD in vitro. Incubating each IpaB fragment with up to a 125-fold excess of IpaD (10 μM) in an aqueous buffer system resulted in essentially no change in polarization, suggesting that no interaction was occurring (Figure 1A, open symbols). Following a 30 min incubation in the presence of 1 mM DOC, however, each labeled IpaB species demonstrated an IpaD-dependent increase in FP (Figure 1A, filled symbols). This change in FP was seen as an initial sharp rise in polarization, indicating that an interaction was occurring. Interestingly, although the apparent K_d values for the interaction between IpaD and $IpaB^{1-226}$ and $IpaB^{11-226}$ in the presence of DOC were below 1 μM, the binding between $IpaB^{28-226}$ and IpaD was significantly weaker, with an apparent K_d of 3.60 μM (Table 1), suggesting that a region within IpaB residues 11–27 together with DOC plays an important role in the interaction between IpaD and IpaB.

The specificity of DOC in promoting the interaction was tested by substituting DHC for DOC. Although structurally similar to DOC, DHC has been shown to neither interact with IpaD nor promote a conformational change within the protein.[13,19] Here, the addition of DHC resulted in no detectable binding of any of the IpaB fragments to IpaD (Supporting Information Figure S1A), supporting a specific DOC-dependent interaction rather than a nonspecific detergent or small-molecule effect. These results are consistent with the inability of DHC exposure to increase *S. flexneri* invasiveness of cultured cells. Whereas exposure to 1 mM DOC substantially increased invasiveness, the addition of DHC had little effect and actually resulted in a slight decrease in invasion (Supporting Information Table S1).

It is worth noting that although all three IpaB peptides could be expressed, purified, and fluorescently labeled at high levels, we found that $IpaB^{11-226}$ was stable longer (by SDS-PAGE) than the $IpaB^{1-226}$ peptide (data not shown). Although comparison of CD spectra of the IpaB peptides does not suggest significant differences in secondary structure (Supporting Information Figure S2 and ref 15), $IpaB^{11-226}$ was selected over $IpaB^{1-226}$ for use in the remainder of the in vitro studies for this observed stability.

Deoxycholate Promotes Binding of $IpaB^{11-226}$ to the IpaD Homologue *Salmonella* SipD but Not *Yersinia* LcrV. To test the specificity for the observed IpaD–IpaB interaction, FP was used to determine the ability of $IpaB^{11-226}$ to bind the homologous T3SS tip proteins SipD from *Salmonella* and LcrV from *Yersinia*. As with IpaD, no change in the polarization of labeled $IpaB^{11-226}$ was observed following a 30 min incubation with either of these recombinant proteins (Figure 1B). The addition of 1 mM DOC failed to promote an interaction between $IpaB^{11-226}$ and LcrV under any observed conditions and is likely attributed to its divergence from IpaD in both primary[24] and tertiary structure.[24,25] Titration of SipD in the

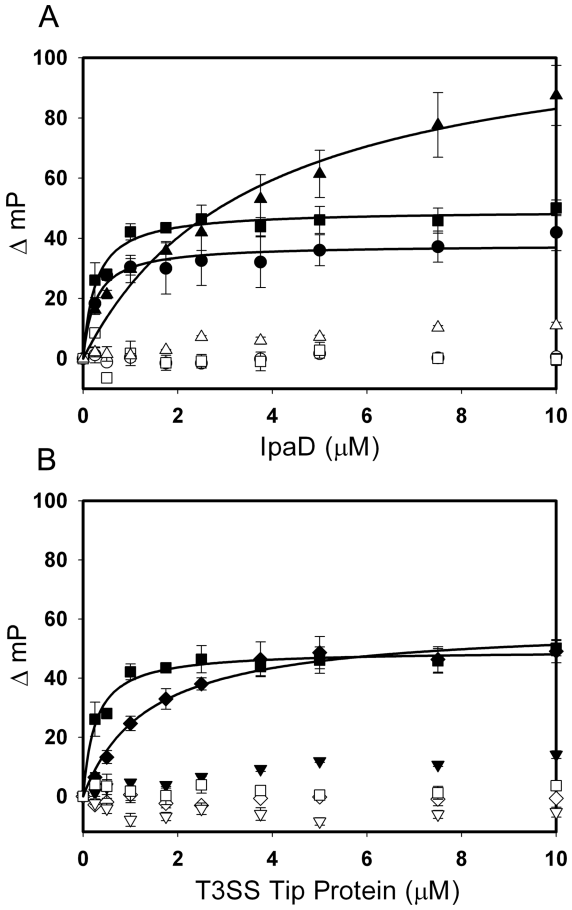

Figure 1. N-terminal IpaB peptides require deoxycholate for optimal interaction with IpaD. (A) Fluorescence polarization of fluorescein-labeled IpaB peptides (80 nM) was monitored as the concentration of IpaD was increased from 0 to 10 μM. IpaD-dependent changes in polarization were monitored for $IpaB^{1-226}$ (●), $IpaB^{11-226}$ (■), and $IpaB^{28-226}$ (▲) following incubation with 1 mM DOC or in the absence of DOC (corresponding open symbols). (B) Fluorescently labeled *Shigella* $IpaB^{11-226}$ was incubated with the T3SS tip proteins from *Salmonella* (SipD, ♦) and *Yersinia* (LcrV, ▼) as well as IpaD (■) in the presence of 1 mM DOC or in the absence of DOC (corresponding open symbols). Each graph is representative of three independent experiments, with error bars indicating the standard deviation of triplicate measurements within a single experiment. The results were fit with a single-site saturation model using SigmaPlot, and the overlaid functions are included for those in which binding occurred ($R^2 > 0.90$).

Table 1. Calculated Dissociation Constants for the *Shigella* T3SS Tip Protein IpaD and N-Terminal Peptides of the Translocator IpaB[a]

IpaB peptide	T3SS tip protein	K_d (μM ± SD)
$IpaB^{1-226}$	IpaD	0.78 ± 0.43
$IpaB^{11-226}$	IpaD	0.39 ± 0.10
$IpaB^{28-226}$	IpaD	3.60 ± 0.37

[a]Apparent dissociation constants were calculated by fitting the polarization data points to a single-site saturation model using SigmaPlot (n = 3 independent measurements).

dx.doi.org/10.1021/bi400755f | *Biochemistry* 2013, 52, 8790–8799

presence of 1 mM DOC, however, resulted in binding (Figure 1B) with an estimated dissociation constant of 1.71 μM, approximately 4-fold weaker than the K_d for the interaction between IpaD and IpaB$^{11-226}$. Association with SipD might be expected because of similarities in their primary sequences;[24] however, the IpaB and SipB N-terminal regions differ rather substantially with regard to sequence despite having notable structural similarity.[14] Although weaker than the IpaD–IpaB$^{11-226}$ interaction, the SipD–IpaB$^{11-226}$ interaction exhibits a similar specificity for DOC because DHC fails to promote binding between SipD and IpaB$^{11-226}$ (Supporting Information Figure S1B). Although DOC binding to SipD with a concomitant conformational change has been reported by others,[26,27] there has not been a direct physiological link between DOC and changes in the *Salmonella* T3SA needle tip composition. In fact, growth in DOC decreases the invasiveness of *Salmonella* in part because of a downregulation of gene expression.[28] Interestingly, short-term (1 min) exposure of a midlog culture to this bile salt also results in a decrease in invasion phenotype, which cannot be entirely contributed to a downregulation of gene expression (data not shown).

Intermolecular FRET Provides Additional Insight into the Association of IpaD with the IpaB N Terminus. Förster resonance energy transfer (FRET) was measured between the CPM-labeled native cysteine (residue 322) of IpaD and the fluorescein-labeled cysteine residue introduced individually into each of four positions within IpaB$^{11-226}$ (S107C, S120C, S128C, and S149C) (Figure 2, panels A and B, respectively). The introduction of each of these cysteine mutations had little impact on secondary structure/stability of the IpaB$^{11-226}$ (Supporting Information Figure S2), and each mutation gave rise to a readily detectable invasive phenotype when introduced into full-length IpaB and expressed in *S. flexneri* SF620 (Supporting Information Table S2). FTIR analysis was used to compare the relative structure structural composition of unlabeled and fluorescein-labeled IpaB$^{11-226}$ S128C (Supporting Information Figure S3).[24,29] No difference in overall protein structure was detected, suggesting that the addition of the fluorescein probe does not have an adverse effect on the protein structure. FRET efficiency between the donor-labeled IpaD and each of the acceptor-labeled IpaB$^{11-226}$ mutants was determined by quantifying the decrease in donor fluorescence in the presence of a FRET acceptor (Figure 2C). The measured energy-transfer efficiencies between the donor-labeled IpaD and all of the acceptor-labeled IpaB$^{11-226}$ cysteine mutants were minimal in the absence of DOC, which is consistent with the absence of an interaction (Table 2). After adding DOC, however, the measured FRET efficiencies increased, indicating the induction of an interaction between IpaD and the IpaB mutants (Table 2). When the *Yersinia* tip protein LcrV was substituted for IpaD in these experiments as a negative control, FRET efficiencies of ≤6.5% were calculated for all conditions, and the addition of 1 mM DOC resulted in a change in FRET efficiencies of no more than 3.3% (data not shown), validating the technique and confirming the lack of interaction between LcrV and IpaB$^{11-226}$ seen in the fluorescence polarization measurements. The FRET efficiencies between the donor-labeled Cys322 of IpaD and acceptor-labeled Cys107 and Cys120 in IpaB$^{11-226}$ were both approximately 33%, and the values decreased to 21.4% and 14.6% as the acceptor moved to Cys128 and Cys149, respectively, (Figure 2A,B and Table 2) suggesting that the donor fluorophore on IpaD was nearest to and approximately equidistant from the acceptor at positions 107 and 120 on IpaB$^{11-226}$. The acceptor probes at positions 128 and 149 then appeared to be located progressively further from the donor probe on IpaD, providing initial insight into the interaction between the proteins.

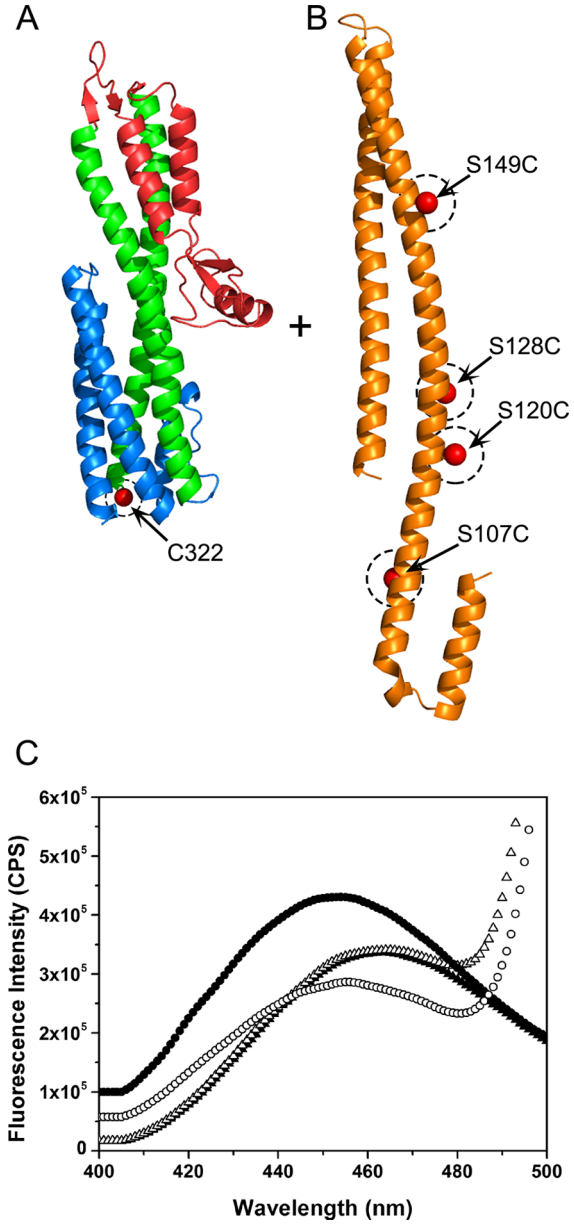

Figure 2. Using FRET to characterize the interaction between IpaD and IpaB. (A) FRET donor probe (CPM) was covalently bound to the thiol of the native IpaD cysteine at position 322. Individual cysteine point mutations were introduced into IpaB$^{11-226}$ at positions 107, 120, 128, and 149 to allow covalent attachment of a FRET acceptor probe (FM) (B). Dashed circles with diameters equal to those of the fluorophores are included at each labeling site. The FRET efficiency between the donor and acceptor was quantified for each acceptor position in the absence and presence of 1 mM DOC on the basis of donor quenching. (C) Representative set of FRET donor emission spectra acquired for coumarin-labeled IpaD in the presence of acceptor-labeled IpaB$^{11-226}$ S107C (△) and unlabeled IpaB$^{11-226}$ S107C (▲). Spectra were reacquired for donor-only and donor-plus-acceptor conditions following the addition of 1 mM DOC (open circles ○ and ●, respectively).

dx.doi.org/10.1021/bi400755f | *Biochemistry* 2013, 52, 8790–8799

Table 2. FRET Efficiencies Characterizing the Interaction between the *Shigella* T3SS Proteins IpaD and IpaB[a]

	FRET efficiency (% ± SD)	
acceptor (fluorescein) location	no DOC	1 mM DOC
$IpaB^{11-226}$ S107C	−0.1 ± 0.0	33.1 ± 1.4
$IpaB^{11-226}$ S120C	8.1 ± 0.1	33.3 ± 0.5
$IpaB^{11-226}$ S128C	7.3 ± 0.1	21.4 ± 0.4
$IpaB^{11-226}$ S149C	8.0 ± 0.1	14.6 ± 0.2

[a]FRET efficiencies were measured between a coumarin donor probe located at the native cysteine (residue 322) in IpaD and a fluorescein acceptor bound to the single cysteine residues mutated in $IpaB^{11-226}$. Results are presented as the percent FRET efficiency ± standard deviation (n = 3 independent measurements).

Intramolecular FRET Implicates DOC in Regulating IpaB Interaction with IpaD via a Conformation Change within the IpaD Distal Domain. Recent EM reconstructions have demonstrated that the IpaD distal domain assumes an upward position within the context of the pentamer formed at the *Shigella* T3SA needle tip.[7] Therefore, we designed an intramolecular FRET system that is sensitive to movement of the IpaD distal domain relative to the native cysteine at the bottom of the central coiled-coil. This would allow us to determine whether association with $IpaB^{11-226}$ is consistent with an upward movement of the IpaD distal domain (Figure 3A). The FRET efficiency between the donor fluorophore at Cys322 (CPM) and the acceptor in the distal domain (FlAsH probe at position TC231) was determined on the basis of the extent of donor quenching as was done for the intermolecular FRET described above. The measured energy-transfer efficiencies followed a dose-dependent decrease with the titration of $IpaB^{11-226}$, indicating that the average position of the IpaD distal domain is directly affected by $IpaB^{11-226}$ binding (Figure 3B). In the absence of DOC, however, titration of $IpaB^{11-226}$ has little effect on the measured intramolecular FRET efficiencies, supporting the idea that DOC promotes a stable IpaD/$IpaB^{11-226}$ interaction. Addition of 5 μM LcrV in place of $IpaB^{11-226}$ failed to produce a change in intramolecular FRET efficiency in either the presence or absence of DOC, indicating a level of specificity for IpaB (data not shown). Moreover, fitting the FRET efficiencies as a function of $IpaB^{11-226}$ concentration (1 mM DOC) to a Hill1 binding model with an adjusted R^2 value of 0.990 allowed us to calculate an apparent K_d value of 365 nM. The striking similarity of the K_d determined here and the K_d determined by FP (378 nM) suggests that the location of the IpaD distal domain is not only linked to the binding of IpaB but that the correlation can be used as a direct measure of interaction. It is worth noting that although this method for measuring FRET efficiencies provides a reliable tool sensitive to angstrom-level structural changes in the protein conformation, absolute FRET efficiencies and distances are difficult to quantify. This is evident because the FRET efficiencies reported here are approximately 20% lower than those reported previously;[13] however, the addition of DOC once again resulted in a measured decrease in FRET efficiency that was exaggerated upon the binding of $IpaB^{11-226}$.

Role of the N-Terminus of IpaB in Formation of the IpaD/IpaB Complex. Although the fluorescence data, as a whole, provide evidence for an interaction between IpaD and the N-terminal fragments of IpaB, the FP data identify a key region in IpaB that may be responsible for a maximal IpaD−IpaB interaction ($IpaB^{11-27}$). Therefore, we used the secondary-structure prediction program PSIPRED[30] to guide in the design of deletion mutants within this region of full-length IpaB for in vivo analysis (Supporting Information Figure S4). Three mutants, $IpaB^{\Delta 12-19}$, $IpaB^{\Delta 12-25}$, and $IpaB^{\Delta 12-27}$, were designed to probe the roles of specific elements of this region by taking into account the predicted secondary-structure components (Supporting Information Figure S4) and maintaining the proposed secretion signal at the extreme N-terminus.[31] $IpaB^{\Delta 12-27}$ mimics the in vitro studies that identified these residues as instrumental in IpaD binding. The $IpaB^{\Delta 12-19}$ and $IpaB^{\Delta 12-25}$ mutants removed the first predicted α-helix and the region containing this helix plus the adjacent coil, respectively. The modified sequences were again analyzed by PSIPRED and although the $IpaB^{\Delta 12-19}$ and $IpaB^{\Delta 12-25}$ mutants resulted in predicted secondary structures consistent with simply removing the defined regions, the $IpaB^{\Delta 12-27}$ mutant was predicted to

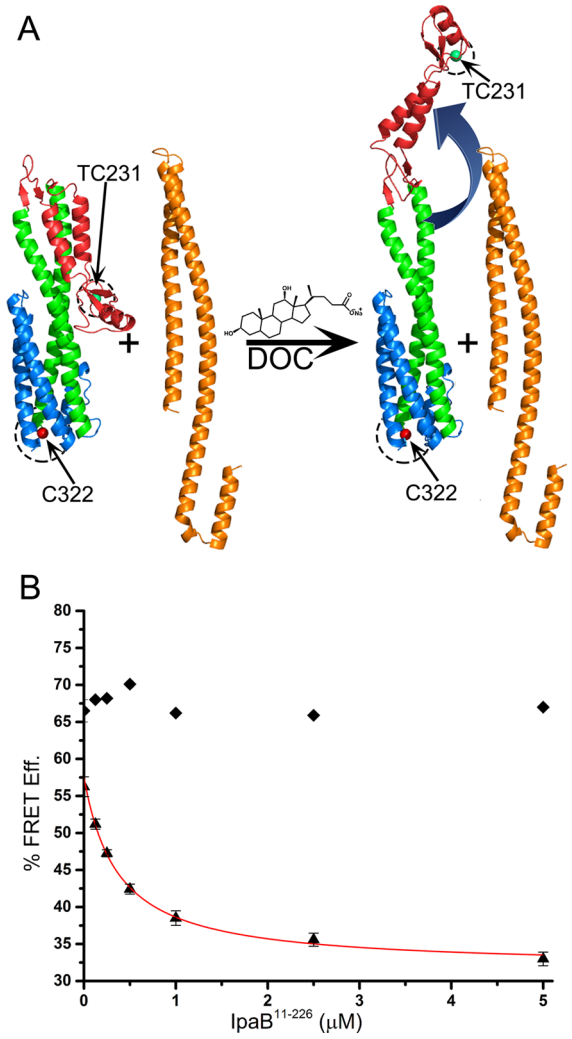

Figure 3. IpaD distal-domain movement accompanies IpaB binding. The locations of FlAsH FRET donor and Alexa Fluor 568 FRET acceptor probes are identified at positions TC231 and Cys322, respectively. Dashed circles with diameters equal to those of the fluorophores are included at each labeling site (A). Plotting IpaD intramolecular FRET efficiency in the absence of DOC (♦) and in the presence of 1 mM DOC (▲) as a function of $IpaB^{11-226}$ indicates a DOC initiated, dose-dependent decrease in FRET efficiency resulting from an increase in distance between the donor and acceptor fluorophores (B), consistent with a movement such as the one illustrated in panel A (right side).

dx.doi.org/10.1021/bi400755f | *Biochemistry* 2013, 52, 8790−8799

extend the second helix an additional five residues toward the N-terminus. The recombinant proteins containing the indicated deletions were purified and analyzed by CD, and the secondary-structure contents estimated using the Dichroweb software package[32,33] including the CDSSTR algorithm.[34] Each of the mutants were found to maintain secondary-structure composition and thermal-stability characteristics similar to wild-type IpaB (Supporting Information Figure S5 and Supporting Information Table S3.

The *ipaB* null *Shigella* strain SF620 was complemented with the above deletion mutants, and the resulting virulence phenotypes were characterized. The uninduced overnight secretion profiles of the T3SA Ipa tip proteins showed that all of the mutants were expressed and secreted at levels similar to SF620 complemented with full-length *ipaB*; however, IpaD and IpaC were hypersecreted with levels similar to those of the *ipaB*-null strain (Figure 4A and Supporting Information Table S4), suggesting impaired secretion control by the IpaB deletion mutants. Analysis of the profiles of the whole cell extracts shows a typical pattern expected when a protein's secretion is uncontrolled, resulting in decreased levels remaining in the cytoplasm (Figure 4B). The ability of the mutant complement strains to lyse erythrocytes through translocon insertion and to invade cultured epithelial cells were tested by hemolysis and gentamicin protection assays, respectively. Each of the mutants exhibited dramatically reduced phenotypes when compared to the full-length-*ipaB* complemented strain (Table 3), suggesting that although the mutants were expressed and secreted Figure 4) they do not form a functioning T3SA tip complex, likely because of the impaired ability of IpaB to interact properly with IpaD.

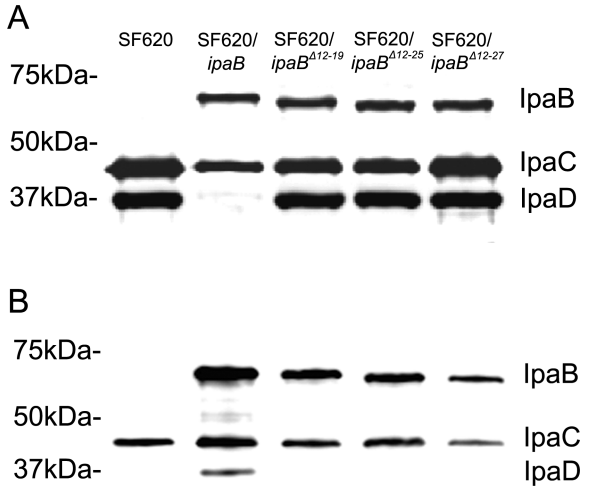

Figure 4. Identification of a region near the IpaB N-terminus necessary for proper *Shigella* T3SS secretion control. Western blots of IpaB, IpaC, and IpaD present in the supernatant (A) and the whole cell extracts (B) of overnight *S. flexneri* cultures.

The ability of IpaB and the IpaB deletion mutants to localize to the bacterial surface as a part of the T3SA was tested using flow cytometry to detect levels of selectively immunolabeled IpaB. All of the strains were grown in the presence of 1 mM DOC to ensure appropriate signaling for IpaB translocation. Five-hundred-thousand events were recorded for each mutant and displayed as a histogram of fluorescence intensity (Figure 5). The wild-type complemented strain exhibited the highest overall fluorescence intensity, whereas the intensity of the IpaB deletion mutants was much lower and is nearly equivalent to those of the IpaB-null strain. Thus, these data further suggest that the deleted regions are involved in maintaining a strong IpaD−IpaB interaction following DOC stimulation.

Table 3. Identifying a Region near the IpaB N-Terminus Required for Proper *Shigella flexneri* Virulence Phenotype

bacterial strain	hemolysis (% ± SD)[a,b]	relative invasion (% ± SD)[c]	
		no DOC	1 mM DOC
ipaB null (SF620)	4.5 ± 0.3	0 ± 0	0 ± 0
SF620 + *ipaB*	100 ± 2.5	100 ± 4	288 ± 6
SF620 $ipaB^{\Delta 12-19}$	5.8 ± 0.3	15 ± 1	21 ± 1
SF620 $ipaB^{\Delta 12-25}$	10.1 ± 1.0	6 ± 1	7 ± 1
SF620 $ipaB^{\Delta 12-27}$	5.9 ± 0.4	1 ± 1	2 ± 1

[a]The ability of the *Shigella* mutants to lyse red blood cells was investigated by a hemolysis assay that spectrophotometrically quantifies the release of hemoglobin from erythrocytes following incubation with the *Shigella*. [b]Results are presented as percent wild-type IpaB ± standard deviation (n = 3 independent measurements). [c]Invasiveness was measured by a standard gentamicin protection assay (see Experimental Procedures), and the results are presented as the percent invasion by *S. flexneri* expressing wild-type IpaB in the absence of DOC. Experiments were repeated in triplicate.

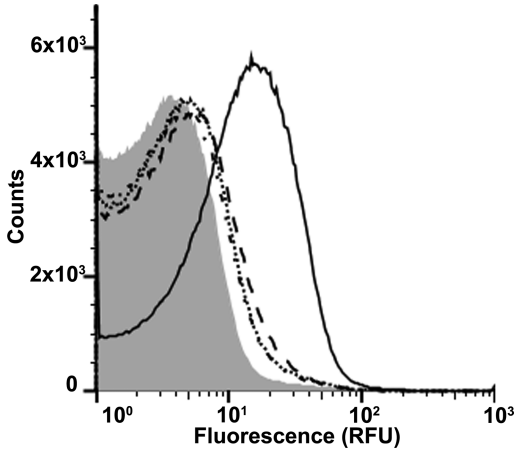

Figure 5. Identification of a region near the IpaB N-terminus necessary for optimal *Shigella* T3SA surface presentation. Fluorescence intensity histograms depicting DOC-induced levels of surface localization of IpaB for the SF620 (*ipaB* null) *S. flexneri* strain (shaded) and those complemented with wild-type IpaB (solid), $IpaB^{\Delta 12-19}$ (dashed), $IpaB^{\Delta 12-25}$ (dotted), and $IpaB^{\Delta 12-27}$ (dash-dot-dash). The decreased levels of the IpaB mutants compared to wild-type are consistent with the in vitro experiments, suggesting that this region near the N-terminus plays an important role in proper IpaD−IpaB interaction and T3SA localization.

DISCUSSION

Incubation of *Shigella* with the bile salt deoxycholate promotes recruitment of IpaB to the maturing T3SA needle tip, which correlates with an enhanced ability of the bacteria to invade cultured epithelial cells.[9] This and other work clearly define IpaD as an important regulator of type III secretion from its position at the *Shigella* T3SA needle tip.[35,36] Nevertheless, until now there has been no demonstration of a direct interaction between the *Shigella* tip protein IpaD and the first hydrophobic translocator IpaB. In this study, we used fragments from the N-terminus of IpaB to demonstrate this interaction, its depend-

dx.doi.org/10.1021/bi400755f | *Biochemistry* 2013, 52, 8790−8799

ence on DOC, and the involvement of a structural change in the IpaD distal domain using complementary fluorescence spectroscopy methods. Initially, FP measurements confirmed that DOC is required for the tested IpaB fragments to bind with IpaD, supporting the proposal that a DOC-induced conformational change in IpaD has a role in promoting stable maintenance of IpaB at the T3SA needle tip.[9,12,13] Intermolecular FRET measurements between a donor probe on IpaD and an acceptor at each of four individual sites on IpaB$^{11-226}$ then suggested that the N-terminal region of the coiled-coil in the solved structure of IpaB resides near the "bottom" of the IpaD coiled-coil (Figure 2). The intramolecular FRET results identified IpaB$^{11-226}$-dependent changes in FRET efficiency consistent with the IpaD distal domain moving further away from the C-terminus of IpaD (flipping upward) upon binding IpaB$^{11-226}$. This movement appears to be needed to accommodate proper interaction with IpaB, possibly by providing IpaB$^{11-226}$ access to previously inaccessible contact points (Figure 3A). Although the precise role of DOC in this interaction and the resulting movement of the distal domain remain unclear, previous work[13] together with these findings suggests that the IpaD distal-domain location relative to the C-terminal cysteine is sensitive to DOC exposure and that this is exacerbated by the subsequent interaction with IpaB.

We also found through the initial FP studies that IpaB residues 11−27 play an important role in optimal binding to IpaD. We were able to confirm the importance of this region in vivo and to narrow down further the region responsible by creating deletion mutants and characterizing the resulting phenotype in *S. flexneri*. Hemolysis and invasion assays showed that loss of this region is detrimental to *Shigella* virulence activities even though the protein was expressed at wild-type levels, secreted through the T3SA (Figure 4), and copurified with IpgC when coexpressed in *E. coli* (data not shown). Consistent with these results, fluorescence immunolabeling of *Shigella* suggested that the IpaB mutants localized to the *Shigella* surface (T3SA) much less efficiently than the wild-type protein (Figure 5), likely a result of the described deficiency in IpaD−IpaB interaction. Furthermore, it is worth noting that although IpaB residues 11−27 appear essential for optimum IpaD interaction and *Shigella* virulence mechanisms, we recently reported that a site within the N-terminal 27 residues of IpaB is also necessary for optimal IpaB binding of its chaperone IpgC.[15] Together, these studies suggest that IpaD and IpgC share an overlapping binding region near the N-terminus of IpaB, which acts to prevent a premature IpaD−IpaB interaction in the bacterial cytoplasm. Unfortunately, we could not directly address whether IpgC and IpaD binding to the IpaB N-terminal domain is competitive because although DOC is required for binding to IpaD, its detergent properties favor dissociation of the IpaB−IpgC heterodimer (data not shown).

From the data presented here, we propose an in vitro model in which exposure of IpaD to DOC induces a conformational change that generates the flexibility needed for the distal domain to move from the position observed in the IpaD crystal structure to permit the IpaD and IpaB coiled-coil cores to align parallel with one another. This is proposed to mimic the in vivo interaction where DOC induces flexibility within the IpaD needle tip pentamer that allows the individual five distal domains (already in an up position) to open up to allow IpaB to move to a position where it is now surface exposed. Although it seems unlikely that the sole driving force for interaction between these two large proteins is a short peptide sequence near the N-terminus of IpaB, both in vitro and in vivo studies presented here suggest that a region as small as that from residues 12−19 in IpaB plays a crucial role in optimizing this interaction. Further investigation into the nature of this interaction, the proposed events leading up to this interaction, and its role in T3SA maturation is needed to understand fully how needle tip maturation occurs and its contribution to *Shigella* virulence; however, results from this study now provide a platform to address these questions.

■ ASSOCIATED CONTENT

Ⓢ Supporting Information

Fluorescence polarization binding curves comparing the effect of DOC and DHC on IpaB$^{11-226}$ interaction with T3SS tip proteins, circular dichroism characterization of IpaB$^{11-226}$ and engineered cysteine point mutants, PSIPRED secondary-structure predictions for N-terminal IpaB deletion mutants, FTIR analysis of fluorescein-bound and unlabeled IpaB$^{11-226}$ S128C, circular dichroism characterization of IpaB N-terminal deletion mutants, effect of DOC and DHC on *S. flexneri* invasion phenotype, invasion phenotype of IpaB engineered cysteine point mutants, DichroWeb secondary-structure prediction results for IpaB N-terminal deletion mutants, and quantification of uninduced secretion by *S. flexneri* expressing IpaB N-terminal deletion mutants. This material is available free of charge via the Internet at http://pubs.acs.org.

■ AUTHOR INFORMATION

Corresponding Author

*Tel.: 405-744-4600; E-mail: wendy.picking@okstate.edu.

Funding

This work was supported by funding to W.L.P. (NIH grant R01 AI067858), W.D.P. (Oklahoma Health Research Program Funding HR10-128S), N.E.D. (NIH grant K22 AI099086), and W.D.P. (NIH grants R21 AI090149 and R01 AI099489). M.K.P. was supported by the Oklahoma State University Niblack Research Scholars Program.

Notes

The authors declare no competing financial interest.

■ ACKNOWLEDGMENTS

We thank Brian V. Geisbrecht for critical reading of the manuscript.

■ ABBREVIATIONS USED

IpaD, invasion plasmid antigen D; T3SS, type III secretion system; T3SA, type III secretion apparatus; DOC, deoxycholate; PMSF, phenylmethylsulfonyl fluoride; DHC, dehydrocholate; CD, circular dichroism; FRET, Förster resonance energy transfer; FP, fluorescence polarization; FTIR, Fourier-transform infrared spectroscopy; CPM, 7-diethylamino-3-(4′-maleimidylphenyl)-4-methylcoumarin; FM, fluorescein maleimide; TCEP, tris(2-carboxyethyl)phosphine; BME, β-mercaptoethanol; DMF, *N*′,*N*′-dimethylformamide; FlAsH-EDT$_2$, fluorescein-containing biarsenical reagent that coordinates with the tetracysteine motif CCPGCC; LcrV, low calcium response T3SA needle tip protein from *Yersinia*; SipD, *Salmonella* invasion protein D

REFERENCES

(1) Kotloff, K. L., Nataro, J. P., Blackwelder, W. C., Nasrin, D., Farag, T. H., Panchalingam, S., Wu, Y., Sow, S. O., Sur, D., Breiman, R. F., Faruque, A. S., Zaidi, A. K., Saha, D., Alonso, P. L., Tamboura, B., Sanogo, D., Onwuchekwa, U., Manna, B., Ramamurthy, T., Kanungo, S., Ochieng, J. B., Omore, R., Oundo, J. O., Hossain, A., Das, S. K., Ahmed, S., Qureshi, S., Quadri, F., Adegbola, R. A., Antonio, M., Hossain, M. J., Akinsola, A., Mandomando, I., Nhampossa, T., Acacio, S., Biswas, K., O'Reilly, C. E., Mintz, E. D., Berkeley, L. Y., Muhsen, K., Sommerfelt, H., Robins-Browne, R. M., and Levine, M. M. (2013) Burden and aetiology of diarrhoeal disease in infants and young children in developing countries (the Global Enteric Multicenter Study, GEMS): A prospective, case-control study. *Lancet 13*, 60844–60852.

(2) WHO Initiative for Vaccine Research (IVR) . (2009) *Diarrhoeal diseases*; Report from the WHO IVR: Geneva, Switzerland; http://www.who.int/vaccine_research/diseases/diarrhoeal/en/index6.html.

(3) Kolling, G., Wu, M., and Guerrant, R. L. (2012) Enteric pathogens through life stages. *Front. Cell. Infect. Microbiol. 2*, 114.

(4) Dutta, S., Ghosh, A., Ghosh, K., Dutta, D., Bhattacharya, S. K., Nair, G. B., and Yoshida, S. (2003) Newly emerged multiple-antibiotic-resistant *Shigella dysenteriae* type 1 strains in and around Kolkata, India, are clonal. *J. Clin. Microbiol. 41*, 5833–5834.

(5) Schroeder, G. N., and Hilbi, H. (2008) Molecular pathogenesis of *Shigella* spp.: Controlling host cell signaling, invasion, and death by type III secretion. *Clin. Microbiol. Rev. 21*, 134–156.

(6) Blocker, A., Jouihri, N., Larquet, E., Gounon, P., Ebel, F., Parsot, C., Sansonetti, P., and Allaoui, A. (2001) Structure and composition of the *Shigella flexneri* "needle complex", a part of its type III secreton. *Mol. Microbiol. 39*, 652–663.

(7) Epler, C. R., Dickenson, N. E., Bullitt, E., and Picking, W. L. (2012) Ultrastructural analysis of IpaD at the tip of the nascent MxiH type III secretion apparatus of *Shigella flexneri*. *J. Mol. Biol. 420*, 29–39.

(8) Espina, M., Olive, A. J., Kenjale, R., Moore, D. S., Ausar, S. F., Kaminski, R. W., Oaks, E. V., Middaugh, C. R., Picking, W. D., and Picking, W. L. (2006) IpaD localizes to the tip of the type III secretion system needle of *Shigella flexneri*. *Infect. Immun. 74*, 4391–4400.

(9) Olive, A. J., Kenjale, R., Espina, M., Moore, D. S., Picking, W. L., and Picking, W. D. (2007) Bile salts stimulate recruitment of IpaB to the *Shigella flexneri* surface, where it colocalizes with IpaD at the tip of the type III secretion needle. *Infect. Immun. 75*, 2626–2629.

(10) Dickenson, N. E., Choudhari, S. P., Adam, P. R., Kramer, R. M., Joshi, S. B., Middaugh, C. R., Picking, W. L., and Picking, W. D. (2013) Oligomeric states of the *Shigella* translocator protein IpaB provide structural insights into formation of the type III secretion translocon. *Protein Sci. 22*, 614–627.

(11) Epler, C. R., Dickenson, N. E., Olive, A. J., Picking, W. L., and Picking, W. D. (2009) Liposomes recruit IpaC to the *Shigella flexneri* type III secretion apparatus needle as a final step in secretion induction. *Infect. Immun. 77*, 2754–2761.

(12) Barta, M. L., Guragain, M., Adam, P., Dickenson, N. E., Patil, M., Geisbrecht, B. V., Picking, W. L., and Picking, W. D. (2012) Identification of the bile salt binding site on IpaD from *Shigella flexneri* and the influence of ligand binding on IpaD structure. *Proteins 80*, 935–945.

(13) Dickenson, N. E., Zhang, L., Epler, C. R., Adam, P. R., Picking, W. L., and Picking, W. D. (2011) Conformational changes in IpaD from *Shigella flexneri* upon binding bile salts provide insight into the second step of type III secretion. *Biochemistry 50*, 172–180.

(14) Barta, M. L., Dickenson, N. E., Patil, M., Keightley, A., Wyckoff, G. J., Picking, W. D., Picking, W. L., and Geisbrecht, B. V. (2012) The structures of coiled-coil domains from type III secretion system translocators reveal homology to pore-forming toxins. *J. Mol. Biol. 417*, 395–405.

(15) Adam, P. R., Patil, M. K., Dickenson, N. E., Choudhari, S., Barta, M., Geisbrecht, B. V., Picking, W. L., and Picking, W. D. (2012) Binding affects the tertiary and quaternary structures of the *Shigella* translocator protein IpaB and its chaperone IpgC. *Biochemistry 51*, 4062–4071.

(16) Lokareddy, R. K., Lunelli, M., Eilers, B., Wolter, V., and Kolbe, M. (2010) Combination of two separate binding domains defines stoichiometry between type III secretion system chaperone IpgC and translocator protein IpaB. *J. Biol. Chem. 285*, 39965–39975.

(17) Menard, R., Sansonetti, P. J., and Parsot, C. (1993) Nonpolar mutagenesis of the ipa genes defines IpaB, IpaC, and IpaD as effectors of *Shigella flexneri* entry into epithelial cells. *J. Bacteriol. 175*, 5899–5906.

(18) Garcia, B. L., Summers, B. J., Lin, Z., Ramyar, K. X., Ricklin, D., Kamath, D. V., Fu, Z. Q., Lambris, J. D., and Geisbrecht, B. V. (2012) Diversity in the C3b [corrected] contact residues and tertiary structures of the staphylococcal complement inhibitor (SCIN) protein family. *J. Biol. Chem. 287*, 628–640.

(19) Stensrud, K. F., Adam, P. R., La Mar, C. D., Olive, A. J., Lushington, G. H., Sudharsan, R., Shelton, N. L., Givens, R. S., Picking, W. L., and Picking, W. D. (2008) Deoxycholate interacts with IpaD of *Shigella flexneri* in inducing the recruitment of IpaB to the type III secretion apparatus needle tip. *J. Biol. Chem. 283*, 18646–18654.

(20) Kaniga, K., Trollinger, D., and Galan, J. E. (1995) Identification of two targets of the type III protein secretion system encoded by the inv and spa loci of *Salmonella typhimurium* that have homology to the *Shigella* IpaD and IpaA proteins. *J. Bacteriol. 177*, 7078–7085.

(21) Mueller, C. A., Broz, P., Muller, S. A., Ringler, P., Erne-Brand, F., Sorg, I., Kuhn, M., Engel, A., and Cornelis, G. R. (2005) The V-antigen of *Yersinia* forms a distinct structure at the tip of injectisome needles. *Science 310*, 674–676.

(22) Lakowicz, J. R. (2006) *Principles of Fluorescence Spectroscopy*, 3rd ed., Springer, New York.

(23) Dickenson, N. E., and Picking, W. D. (2012) Forster resonance energy transfer (FRET) as a tool for dissecting the molecular mechanisms for maturation of the *Shigella* type III secretion needle tip complex. *Int. J. Mol. Sci. 13*, 15137–15161.

(24) Espina, M., Ausar, S. F., Middaugh, C. R., Baxter, M. A., Picking, W. D., and Picking, W. L. (2007) Conformational stability and differential structural analysis of LcrV, PcrV, BipD, and SipD from type III secretion systems. *Protein Sci. 16*, 704–714.

(25) Derewenda, U., Mateja, A., Devedjiev, Y., Routzahn, K. M., Evdokimov, A. G., Derewenda, Z. S., and Waugh, D. S. (2004) The structure of *Yersinia pestis* V-antigen, an essential virulence factor and mediator of immunity against plague. *Structure 12*, 301–306.

(26) Chatterjee, S., Zhong, D., Nordhues, B. A., Battaile, K. P., Lovell, S., and De Guzman, R. N. (2011) The crystal structures of the *Salmonella* type III secretion system tip protein SipD in complex with deoxycholate and chenodeoxycholate. *Protein Sci. 20*, 75–86.

(27) Wang, Y., Nordhues, B. A., Zhong, D., and De Guzman, R. N. (2010) NMR characterization of the interaction of the *Salmonella* type III secretion system protein SipD and bile salts. *Biochemistry 49*, 4220–4226.

(28) Prouty, A. M., and Gunn, J. S. (2000) *Salmonella enterica* serovar typhimurium invasion is repressed in the presence of bile. *Infect. Immun. 68*, 6763–6769.

(29) Middaugh, C. R., Mach, H., Ryan, J. A., Sanyal, G., and Volkin, D. B. (1995) Infrared spectroscopy. *Methods Mol. Biol. 40*, 137–156.

(30) Jones, D. T. (1999) Protein secondary structure prediction based on position-specific scoring matrices. *J. Mol. Biol. 292*, 195–202.

(31) Harrington, A. T., Hearn, P. D., Picking, W. L., Barker, J. R., Wessel, A., and Picking, W. D. (2003) Structural characterization of the N terminus of IpaC from *Shigella flexneri*. *Infect. Immun. 71*, 1255–1264.

(32) Lobley, A., Whitmore, L., and Wallace, B. A. (2002) DICHROWEB: An interactive website for the analysis of protein secondary structure from circular dichroism spectra. *Bioinformatics 18*, 211–212.

(33) Whitmore, L., and Wallace, B. A. (2004) DICHROWEB: An online server for protein secondary structure analyses from circular dichroism spectroscopic data. *Nucleic Acids Res. 32*, W668–673.

(34) Johnson, W. C. (1999) Analyzing protein circular dichroism spectra for accurate secondary structures. *Proteins 35*, 307–312.

(35) Schiavolin, L., Meghraoui, A., Cherradi, Y., Biskri, L., Botteaux, A., and Allaoui, A. (2013) Functional insights into the *Shigella* type III needle tip IpaD in secretion control and cell contact. *Mol. Microbiol. 88*, 268−282.
(36) Roehrich, A. D., Guillossou, E., Blocker, A. J., and Martinez-Argudo, I. (2013) *Shigella* IpaD has a dual role: Signal transduction from the type III secretion system needle tip and intracellular secretion regulation. *Mol. Microbiol. 87*, 690−706.